The Journals of Gerontology, Series A: Biological Sciences and Medical Sciences, 2025, **80**(7), glaf081
https://doi.org/10.1093/gerona/glaf081
Advance access publication: 15 April 2025
Original Article

Cardiovascular-Derived Circulating Cell-Free DNA Fragments Are Associated With Frailty and Increased Cardiovascular Events in Older Adults

Lolita S. Nidadavolu, MD, PhD,[1,†] David W. Sosnowski, PhD,[2,†] Nikita Sivakumar, BS,[3,†] Alessandra Merino Gomez, BS,[1] Yuqiong Wu, MD,[1] Thomas Laskow, MD,[1] Taylor Bopp, BS,[1] Nicholas Milcik, BA,[1] Anne Le, MD, HDR,[4] Cissy Zhang, BS,[4] Pratik Khare, MS,[4] Andrea Zammit, PhD,[5] Francine Grodstein, PhD,[5] Jeremy D. Walston, MD,[1] David A. Bennett, MD,[5] Rasika A. Mathias, PhD,[6] Jude M. Phillip, PhD,[3,7,8] Brion S. Maher, PhD,[2] Esther S. Oh, MD, PhD,[1] and Peter M. Abadir, MD[1,*]

[1]Division of Geriatrics and Gerontology, Johns Hopkins University School of Medicine, Baltimore, Maryland, USA.
[2]Department of Mental Health, Johns Hopkins Bloomberg School of Public Health, Baltimore, Maryland, USA.
[3]Department of Biomedical Engineering, Whiting School of Engineering, Johns Hopkins University, Baltimore, Maryland, USA
[4]Gigantest, Baltimore, Maryland, USA.
[5]Rush Alzheimer's Disease Center, Rush University Medical Center, Chicago, Illinois, USA.
[6]Department of Medicine, Johns Hopkins University School of Medicine, Baltimore, Maryland, USA.
[7]Department of Chemical and Biomolecular Engineering, Institute for Nanobiotechnology, Whiting School of Engineering, Johns Hopkins University, Baltimore, Maryland, USA.
[8]Department of Oncology, Sidney Kimmel Comprehensive Cancer Center, Johns Hopkins University School of Medicine, Baltimore, Maryland, USA.

*Address correspondence to: Peter M. Abadir, MD. E-mail: pabadir1@jhmi.edu
[†]These authors contributed equally to this work.

Decision Editor: Gustavo Duque, MD, PhD (Biological Sciences Section)

Abstract

Increased cellular damage in aging tissues releases circulating cell-free genomic DNA (ccf-gDNA) into the bloodstream, and these fragments are associated with a higher risk of frailty and dementia. We hypothesized that identifying the tissue of origin for ccf-gDNA using methylation signatures can distinguish subgroups of participants with distinct clinical outcomes, biological aging rates, and energy use. Serum ccf-gDNA from 181 participants in the Religious Orders Study or Rush Memory and Aging Project (ROS-MAP) was assessed for DNA methylation at one timepoint using the Illumina MethylationEPIC array. Clinical outcomes 6 years after ccf-gDNA measurement were determined for the following: frailty, cognitive test scores, and cardiovascular disease. Hierarchical clustering identified major clusters based on the predominance of ccf-gDNA source: cardiovascular, erythrocyte progenitor, and immune cell. Participants with cardiovascular-enriched ccf-gDNA (CV ccf-gDNA) had higher rates of myocardial infarction (39%) at the last study visit compared to other subgroups (Immune ccf-gDNA: 21%; Erythrocyte ccf-gDNA: 23%), and similar findings were observed for congestive heart disease and stroke. There were no significant associations between cognitive test scores and ccf-gDNA subgroups. Individuals with CV ccf-gDNA demonstrated 3.1 times higher odds of being frail compared to the other groups and showed increased epigenetic age acceleration for the fragments compared to the other subgroups, indicating that this group was enriched with ccf-gDNA originating from older cells. The CV ccf-gDNA subgroup exhibited dysregulation of glycine and serine metabolism and pathways integral to cardiovascular health, endothelial function, and inflammation. We demonstrate that ccf-gDNA methylation patterns can detect high-turnover tissues and identify older adults at higher risk of frailty and cardiovascular disease.

Keywords: Cardiovascular, Coronary heart disease, DNA, DNA methylation

Aging is a complex process characterized by accumulated cellular damage, which can lead to dysfunctional cell processes and an increased risk of cell death (1). Cell death, through mechanisms such as apoptosis, necrosis, and autophagy, plays a crucial role in the physical and cognitive decline observed in aging individuals (2–4). These mechanisms are tightly regulated under normal physiological conditions to maintain cellular homeostasis but can become dysregulated with aging, leading to the loss of cells in critical tissues and organs and, consequently, functional impairments that contribute to physical and cognitive decline (5,6). Circulating cell-free genomic DNA (ccf-gDNA) fragments are small, double-stranded, single-stranded, and circular DNA molecules released into the bloodstream following cell death and turnover processes and

Received: October 11 2024; Editorial Decision Date: April 5 2025.

are both passively and actively secreted into circulation (7). These fragments have garnered significant interest as potential minimally invasive biomarkers for age-associated diseases such as Alzheimer's disease and other forms of dementia (8,9). Elevated levels of ccf-gDNA in serum have been associated with poorer physical and cognitive health outcomes (10). However, key questions remain: Which tissues primarily release these fragments, do their sources differ between individuals with and without cognitive and physical decline, and are differences in energy utilization and metabolic pathways associated with fragments from different sources?

Given the genomic origin, a notable characteristic of ccf-gDNA is the presence of DNA methylation (DNAm) (11) patterns, or "signatures," that are unique to specific tissues and change with age, thereby serving as a molecular fingerprint for the cellular origin of the DNA. Identifying the tissue of origin for ccf-gDNA is an important step in determining differential cell death and turnover rates in different tissues. This information may prove critical to understanding the molecular mechanisms underlying aging and age-related diseases, as well as facilitating early detection, monitoring, and response to treatment based on an individual's unique molecular signature (12–15). In addition to its potential for identifying cell composition (here, the source tissue of origin for the ccf-DNA), DNAm is also the basis for calculating biological age using epigenetic clocks, which are computed based on specific sets of age-related CpGs (16). Although chronological age is a strong predictor of many age-related diseases, it does not account for the great degree of heterogeneity seen in aging and varied responses in adults of the same age to a common stressor (eg, infection or surgery). The field of geroscience has, therefore, identified biomarkers that can better convey this heterogeneity and provide a biological age for an individual, one of which is the development of epigenetic clocks. The first epigenetic clock, developed using saliva-derived DNA, introduced the concept of biological age—a quantitative measure of gene–environment interactions, as opposed to chronological age, which only accounts for the passage of time (17).

Two epigenetic clocks hold relevance for characterizing ccf-gDNA and examining its association with physical and cognitive decline. The Hannum clock (18), derived from blood-based DNA, consists of 71 distinct CpGs and strongly predicts aging-related outcomes. Hannum age is particularly relevant in the context of physical and cognitive decline (19). The GrimAge clock is a strong predictor of mortality, making it a valuable tool for evaluating mortality risk in various clinical settings (20,21).

It is important to note that these epigenetic clocks were developed and validated using DNA extracted from live cells. In contrast, studying the biological age of DNA fragments from dead cells could potentially offer new insights into the intricacies of cellular aging and death with implication in understanding human resilience and reserve. Additionally, by incorporating serum metabolomics, organism-wide metabolic changes and altered energy pathway utilization can be identified and linked to tissue-specific cell death processes and biological age of ccf-gDNA fragments. This integrated approach has the potential to significantly advance our understanding of disease progression, facilitate early detection, and enable personalized therapeutic interventions, ultimately improving patient outcomes across a broad range of medical conditions.

In this study, we collected serum ccf-gDNA fragments from 181 older adults and analyzed them using the Illumina MethylationEPIC array to identify tissue source and estimate epigenetic clocks. We examined cross-sectional and longitudinal associations between different clusters of individuals grouped by tissue source of ccf-gDNA and clinical diagnoses. We also compared the epigenetic clock estimates from the ccf-gDNA to cellular DNA from helper T cells (CD4 cells) to compare the biological age of dead and living cells. Additionally, we used targeted metabolomics to identify circulating metabolic changes associated with different ccf-gDNA fragment tissue sources.

Method

Sample Description

Our study used stored serum samples from participants ($N = 181$) in the Religious Orders Study (ROS) or Rush Memory and Aging Project (MAP), collectively known as ROS-MAP (22,23), to extract cf-gDNA. A subset of these participants ($n = 39$) had previously undergone CD4 cell isolation from whole blood samples and subsequent DNA isolation. The ROS, initiated in 1994, includes nuns, priests, and brothers from across the United States. The MAP, launched in 1997, comprises community-dwelling older adults from the greater Chicago area. Both studies are analytic cohort studies of risk factors for common chronic diseases and conditions of aging in which all participants are organ donors (22). Both studies received approval from the Institutional Review Board of Rush University Medical Center and adhered to the Declaration of Helsinki. Participants provided a signed informed consent, Anatomic Gift Act, and repository consent for sharing data for research purposes. Annual assessments for all participants collect data on various physical, psychological, medical, and biological factors (22,23). For this study, serum samples were chosen from one timepoint close to study enrollment for ccf-gDNA measurement, and participants had, on average, 6 years of follow-up for clinical measures.

Biological Measures

Circulating cell-free genomic DNA

We measured ccf-gDNA in serum samples using digital PCR with the ThermoFisher QuantStudio 3D Digital PCR system using the protocol previously described (10). Briefly, serum was diluted in phosphate-buffered saline (pH 7.4), heat denatured, and then vortexed to break up the pellet. Following centrifugation, the supernatant was used for digital PCR. Primers targeting RPPH1 (Qiagen) amplified circulating fragments using the following thermocycling conditions: 95°C for 120 seconds, and 40 cycles of 95°C for 15 seconds and 55°C for 45 seconds, followed by imaging. Amplification thresholds were applied, and data were analyzed using QIAcuity Software Suite 2.5.0.

ccf-gDNA methylation

We purified ccf-gDNA from 450 µL of serum using the QIAamp Circulating Nucleic Acid Kit (Qiagen) and eluted it in 40 µL of the provided elution buffer. We analyzed bisulfite-treated purified ccf-gDNA using the Illumina Infinium MethylationEPIC BeadChip (24), which contains over 850,000 CpG sites, including more than 90% of those in the previous 450K BeadChip. The EPIC BeadChip assesses an additional ~400,000 CpG sites and includes over 350,000 sites at potential enhancer regions. We processed raw red and green channel

intensity files according to the pipeline previously outlined (15) to ensure accurate results for deconvolution. CpG sites were filtered out based on the following criteria: represented by less than 3 beads, detection *p*-value > .01, or mapped to a sex chromosome. We performed background correction and normalization using the *preprocessIllumina* function, which eliminates background noise based on internal control probes and normalizes samples to a predetermined control. This resulted in 423,455 CpG sites for deconvolution analysis per the analytic pipeline described in Moss et al. (15).

Deconvolution of ccf-gDNA methylation

DNAm patterns of cf-gDNA were used to deconvolve the samples and estimate tissue of origin. Sample deconvolution was carried out using the pipeline described by Moss et al. (15), which is publicly available on GitHub (https://github.com/nloyfer/meth_atlas). Using 423,455 CpG sites from the DNAm preprocessing, and a reference atlas of 7891 CpG sites, we obtained estimates for 25 possible unique tissue types of origin for the ccf-gDNA. The estimates, represented as proportions on a scale of 0–1, were converted to percentages and used as predictors for inferential analyses.

CD4 cell DNAm

$CD4^+$ T cells were isolated from frozen peripheral blood mononuclear cells (PBMCs) from a subset of 39 ROS-MAP participants (as part of other research) using magnetic-activated cell sorting (MACS), and final samples were at least 95% pure for $CD4^+$ T cells, as assessed by flow cytometry. AllPrep DNA/RNA Micro kit was used to isolate blood DNA, according to manufacturer's instructions. The Illumina InfiniumHumanMethylation450 platform was used to generate DNAm profiles. Additional details of the protocol are detailed in Yu et al. (25) $CD4^+$ T-cell methylation data were provided by the RADC Data Hub.

Epigenetic age

We calculated biological age using 2 epigenetic clocks for ccf-gDNA (n = 181) and CD4 samples (n = 39) using the Horvath DNAm Age online calculator: HannumAge (18) and GrimAge (20). The calculator (https://dnamage.genetics.ucla.edu) provides epigenetic age acceleration estimates by regressing epigenetic age on chronological age. The residuals serve as continuous indicators of accelerated aging, with positive values reflecting accelerated aging and negative values indicating decelerated aging compared to chronologic age. As some of the CD4 and cf-gDNA samples were collected at different timepoints (within 1–2 years from each other), we used multivariable linear regression to assess the association between epigenetic age acceleration in cf-gDNA samples and CD4 samples, adjusting for the time between study visits.

Metabolomics

Metabolites were extracted and quantified using the AbsoluteIDQ kit p400 (Biocrates Life Science AG, Innsbruck, Austria). Targeted analyses of 400 total metabolites (including amino acids, biologic amines, polar lipids, and neutral lipids) were performed on Q-Exactive Plus mass spectrometer with a Vanquish UHPLC system (Thermo Fisher, Waltham, MA, USA).

Serum samples (10 µL) were pipetted onto the center of spots in a 96-well Biocrates kit, dried with Eppendorf Vacufuge speedvac, and incubated with 50 µL of 5% PITC reagent for 20 minutes. After drying, 300 µL of 5 mM ammonium acetate in methanol was added to each well, and the plate was incubated for 30 minutes at room temperature (200 rpm). Samples were centrifuged (500*g*, 2 minutes), and 150 µL of each sample was transferred to an empty 96-deep-well plate. The extracts were diluted for liquid chromatography (LC) by adding 150 µL of high-performance liquid chromatography–mass spectrometry (HPLC-MS) grade water and for flow injection analysis (FIA) by adding 250 µL of FIA running solvent (Biocrates solvent diluted with HPLC-MS grade methanol). The LC plate was run first, with 5 µL of each sample injected onto the Biocrates column. The mobile phase consisted of Solvent A (water containing 0.2% formic acid) and Solvent B (acetonitrile containing 0.2% formic acid) with the following gradient: 0–0.25 minutes: 0% B at 0.8 mL/min flow; 1.5 minutes: 12% B at 0.8 mL/min flow; 2.7 minutes: 17.5% B at 0.8 mL/min flow; 4 minutes: 50% B at 0.8 mL/min flow; 4.5 minutes: 95% B at 0.8 mL/min flow; 4.7 minutes: 95% B at 1.0 mL/min flow; 5.1 minutes: 95% B at 1.0 mL/min flow; 5.25 minutes: 0% B at 1.0 mL/min flow; and 5.8 minutes: 0% B at 0.8 mL/min flow. Evaluation of the samples was carried out using the Thermo Fisher XCalibur and Biocrates MetIDQ software. The FIA plate was run with 20 µL injection of each sample directly into the MS with Biocrates FIA solvent diluted with HPLC-MS grade methanol as the mobile phase, with the following flow rate: 0–1.4 minutes: 50 µL/min; 1.6 minutes: 200 µL/min; 2.8 minutes: 200 µL/min; and 3.00 minutes: 50 µL/min. Concentrations were calculated using the MetIDQ software. PITC, ammonium acetate, water, methanol, and acetonitrile (LC-MS grade) were purchased from Sigma Aldrich.

Clinical Measures

Cognitive functioning

A battery of 17 cognitive tests common to both cohorts was conducted at each study visit to assess the following cognitive domains: episodic memory, semantic memory, working memory, perceptual orientation, and perceptual speed (26). Raw scores from the battery of cognitive tests were converted to *z*-scores (M = 0, SD = 1) and averaged to yield a global cognitive function score where higher scores indicate better cognitive functioning. A complete description of each cognitive test can be found in Supplementary Appendix A. Further, we made clinical diagnoses of dementia and its causes, including Alzheimer's dementia, mild cognitive impairment (MCI), and no cognitive impairment (NCI) as previously reported (27–29).

Physical frailty

Participant physical functioning, including frailty, was assessed at each study visit using a battery of 4 tests assessing grip strength, timed walk, body composition, and fatigue (30,31). Raw scores from the battery of tests were converted to *z*-scores and averaged to yield a frailty score where higher scores correspond to greater frailty. A complete description of each assessment used in the frailty composite can be found in Supplementary Appendix B.

Statistical Methods

All statistical analyses were conducted using Python and R statistical software. Below we describe specific statistical tests and hyperparameters associated for each analysis.

CCF-gDNA tissue origin estimation

We obtained estimates of tissue of origin for the ccf-gDNA using the methods outlined previously by Moss et al. (15). Prior to the following statistical analyses, the tissue source data were processed to condense tissues with low occurrence into overarching organ system groups. First, several tissue sources were excluded: neutrophils, thyroid cells, prostate cells, uterus/cervix cells, breast cells, adipocytes, and cortical neurons. Neutrophils were excluded because they comprise a large proportion of the ccf-gDNA and occlude other patient-to-patient differences. The remaining cell types were excluded due to very low occurrence or being a part of sex-dependent organs. The remaining tissue sources were combined into the following organ system groups including: cardiovascular (vascular endothelial cells and left atrial cells), immune (monocytes, natural killer cells, B cells, $CD4^+$ T cells, and $CD8^+$ T cells), erythrocyte (erythrocyte progenitors), digestive (pancreatic beta, acinar, and duct cells, hepatocytes, colon epithelial cells, bladder cells, kidney cells, and upper gastrointestinal tract cells), and respiratory (lung cells and head and larynx cells).

Hierarchical clustering of ccf-gDNA tissue origin

We used the Scipy package in Python to apply hierarchical clustering (specifying a Euclidean distance metric and Ward linkage method) to derive clusters of ccf-gDNA signatures.

Association of ccf-gDNA groups with clinical measures

Statistical tests for comparisons of continuous cognition and frailty indicators between clusters included Kruskal–Wallis tests followed by the Mann–Whitney *U* test for post hoc comparisons with a significance threshold of $p = .05$. Additionally, the prevalence of discrete frailty status (robust, prefrail, and frail) and cognitive status (normal cognition, MCI, and dementia) in patients from each ccf-gDNA group was measured at the time of the visit in which ccf-gDNA was collected and annually until the final visit. These prevalences were compared to an assumed uniform distribution using a chi-squared test. Additionally, the time in years from the ccf-gDNA visit to prefrailty and frailty was assessed for each group. These analyses indicate the time until the first diagnosis of either status. Patients can revert from prefrailty to robust or frailty to prefrailty diagnoses after this preliminary diagnosis. Additional statistical analysis was not conducted due to the limited sample size. Lastly, we used multinomial logistic regression to examine whether clusters identified from hierarchical clustering were associated with discrete frailty status at the serum visit.

Clinical disease prevalence and time-to-event analysis

We assessed the prevalence of several age-related clinical conditions (anemia, cancer, vascular claudication, thyroid disease, diabetes, hypertension, head injury) across the 3 ccf-gDNA patient groups derived from hierarchical clustering. The presence or absence of disease was noted annually and measured at the same visit at which ccf-gDNA was measured. Heatmaps were generated to represent the proportion of patients positive or negative for the disease at the study's final visit. We assessed the statistical significance of deviation from an assumed uniform distribution between negative and positive for each patient group using a chi-squared test. Additionally, the time in years from the visit at which ccf-gDNA was collected to diagnosis with the disease was plotted for each ccf-gDNA group. These graphs assume that patients are negative for the disease until the first time they are marked positive in the database. Along with this assumption, we assume patients are negative for the disease even if there is missing data for visits prior to a positive diagnosis.

Analysis of epigenetic age acceleration

Multivariable linear regression was also used to examine (i) the association between ccf-gDNA groups and epigenetic age acceleration at the serum study visit, adjusting for age at this visit, and (ii) epigenetic age acceleration estimates derived from ccf-gDNA and CD4 cells, adjusting for the time between study visits. To aid in the interpretation of findings from the models examining differences between ccf-gDNA groups, we used epigenetic age acceleration estimates derived from subtracting chronological age from epigenetic age to obtain units in years.

Targeted metabolomic analysis of ccf-gDNA tissue clusters

We used the R-based web tool, MetaboAnalyst R, to compute fold changes of individual metabolites in the cardiovascular group compared to the erythrocyte and immune groups. We also used MetaboAnalyst to conduct metabolite set enrichment analysis to identify perturbed pathways in the cardiovascular ccf-gDNA group with respect to the erythrocyte and immune groups. The MetaboAnalyst algorithm and associated statistical adjustments for multiple comparisons testing were previously published (32). We processed and normalized the data using the SciKit-Learn package in Python prior to feeding the data into MetaboAnalyst. The original metabolite dataset contained 326 metabolites for 181 participants. Metabolites with missing values for >20 (~10%) patients were excluded. We performed KNN imputation using the SciKit-Learn imputer module ($k = 5$ neighbors, Euclidean distance metric) to fill in missing values for the remaining metabolites. These steps led to a processed dataset composed of 203 metabolites. The data were then log (base 10) normalized, and outliers below the first percentile and above the 99th percentiles were removed. Finally, the data were standard scaled. These steps led to a cleaned dataset of 158 patients and 203 metabolites.

Within MetaboAnalyst, the Statistical Analysis (one factor) tool was used to compute fold changes, and the Enrichment Analysis tool was used to conduct metabolite set enrichment analysis. For both tools, the data were read in as a spreadsheet containing processed metabolomic data of either cardiovascular and erythrocyte subgroups (for comparing participants enriched with cardiovascular ccf-gDNA against a baseline of participants enriched with erythrocyte progenitor ccf-gDNA) or cardiovascular and immune subgroups (for comparing participants enriched with cardiovascular ccf-gDNA against a baseline of participants enriched with immune ccf-gDNA). Metabolites were read in according to their HMDB IDs. Because we processed the data prior to using the MetaboAnalyst tool, no data filtration or normalization was performed within the web tool. For metabolite set enrichment analysis, we used the SMPDB pathway database and included pathways with at least 5 metabolite entries.

Lastly, Pearson correlations were used to assess the relationship between metabolite intensity values and the tissue and organ source of origin for ccf-gDNA. Metabolic pathway analysis was then performed on the metabolites that showed significance in correlational analyses.

Results

In this study, we cross-sectionally measured ccf-gDNA in serum samples obtained from 181 older adults using the Illumina MethylationEPIC array to explore associations between ccf-gDNA tissue origins, epigenetic aging, and longitudinal clinical diagnoses. Our investigation included both cross-sectional and longitudinal analyses, comparing fragment sources and epigenetic clock estimates from ccf-gDNA and cellular DNA (PBMCs), alongside metabolomics to identify biomarkers linked to aging and disease states. Table 1 presents the demographic characteristics of the study participants. We obtained serum samples from most of the 181 participants during their first follow-up visit (n = 111; 61%), 1 year after joining the study. The remaining participants provided samples between Visits 2 and 9. At the time of sample collection (ie, index visit), most (n = 113) had normal cognition. However, 62 had MCI, and 6 had Alzheimer's dementia. The study population primarily consisted of females (71%), with 99% identifying as White.

Decoding the Origins of ccf-gDNA in Older Adults

We employed the deconvolution pipeline by Moss et al. (15) to estimate the tissue of origin for ccf-gDNA samples. Supplementary Figure S1 displays the original output from this analysis. Results indicated that, on average, across all samples, 78% of ccf-gDNA originated from neutrophils, as anticipated due to the samples originating from serum. This finding aligns with the patterns observed by Moss et al. (15). Vascular endothelial cells were the next most common cell type of origin (5.3%), followed by other blood cell types (Supplementary Figure S1). We then streamlined the analysis by grouping these tissues into broader organ system-related categories. This approach was taken to reduce the complexity of individual tissue types within an organ, allowing for a more focused examination of organ-specific ccf-gDNA fragment distribution across our cohort.

Unsupervised Hierarchical Clustering Reveals 3 Major CCF-gDNA Subgroups

Building on our analysis of ccf-gDNA origins, we next explored the diversity within our dataset through unsupervised hierarchical clustering. This approach aimed to identify potential patterns or subgroups among participants based on the tissue source signatures of their ccf-gDNA. As shown in Supplementary Figure S1, each participant had a heterogeneous signature of ccf-gDNA tissue sources; therefore, we were curious whether there were emergently similar ccf-gDNA tissue source phenotypes. After processing, we applied hierarchical clustering to the ccf-gDNA organ systems for each patient to derive 3 major, distinct phenotypes (Figure 1B): an Immune ccf-gDNA fragment-enriched subgroup (Immune ccf-gDNA, n = 98), an Erythrocyte progenitor ccf-gDNA fragment-enriched subgroup (Erythrocyte ccf-gDNA, n = 38), and a Cardiovascular ccf-gDNA fragment-enriched subgroup (CV ccf-gDNA, n = 45). The Immune ccf-gDNA subgroup was correlated with lower white blood cell (WBC) counts compared to the CV ccf-gDNA subgroup ($p < .05$) (Supplementary Figure S2); however, there were no significant differences between groups for red blood cell (RBC) count (Supplementary Figure S2). All 3 groups demonstrated similar chronological age and body mass index (Figure 2A, Supplementary Figure S3).

Table 1. Demographic, Cognitive, and Biological Characteristics at Index Visit

	Analytic Sample (N = 181)	Immune Subgroup (n = 98)	Cardiovascular Subgroup (n = 45)	Erythrocyte Subgroup (n = 38)
Age, mean (*SD*)	84.5 (5.5)	84.6 (5.5)	84.5 (5.3)	84.3 (5.8)
Sex (female), *n* (%)	130 (71.8)	69 (70.4)	32 (71.1)	29 (76.3)
Race (White), *n* (%)	179 (98.9)	96 (98.0)	45 (100)	38 (100)
Years of education, median (IQR)	15 (4)	16 (5)	14 (4)	14 (4)
Years of follow-up, median (IQR)	6 (4)	6 (5)	5 (4)	6 (4)
Cognitive status				
NC	113 (62.4)	62 (63.3)	28 (62.2)	23 (60.5)
MCI	62 (34.3)	31 (31.6)	17 (37.8)	14 (36.8)
ADRD	6 (3.3)	5 (5.1)	0 (0)	1 (2.6)
Global cognitive function, *z*-score mean (*SD*)	−0.13 (0.6)	−0.18 (0.6)	−0.10 (0.5)	−0.10 (0.5)
Frailty status, *n* (%)*				
Robust	41 (29.1)	21 (28.8)	8 (20.5)	12 (41.4)
Prefrail	81 (57.4)	42 (57.5)	24 (61.5)	15 (51.7)
Frail	19 (13.5)	10 (13.7)	7 (17.9)	2 (6.9)
Frailty, *z*-score mean (*SD*)	0.29 (0.6)	0.29 (0.6)	0.45 (0.6)	0.09 (0.7)
Biological data				
ccf-gDNA (copies/µL, raw), mean (*SD*)	7.48 (8.12)	5.95 (6.91)	10.80 (8.37)	7.47 (9.61)
ccf-gDNA (copies/µL, purified), mean (*SD*)	0.59 (0.77)	0.60 (0.93)	0.70 (0.58)	0.40 (0.43)
Epigenetic clock acceleration estimate, mean (*SD*)				
HannumAge acceleration	−0.27 (8.53)	−2.21 (7.37)	1.38 (6.25)	2.78 (7.17)
GrimAge acceleration	−0.23 (6.43)	−1.10 (5.02)	2.22 (6.22)	−0.90 (5.70)

Notes: *Data on frailty categories available for n = 141. ADRD = Alzheimer's disease or related dementia; ccf-gDNA = circulating cell-free genomic DNA; IQR = interquartile range; MCI = mild cognitive impairment; NC = normal cognition.

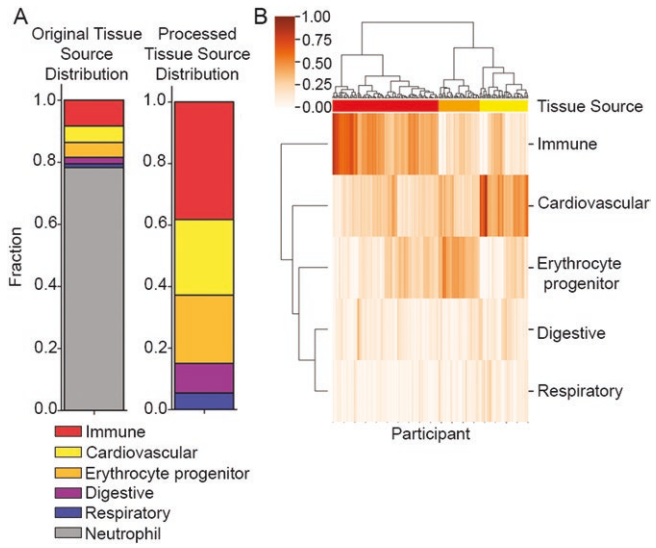

Figure 1. Derivation of distinct patient groups based on circulating cell-free genomic DNA (ccf-gDNA) tissue source. (**A**) Distribution of original and processed tissue sources of ccf-gDNA in our population. The Immune tissue ccf-gDNA fragment-enriched subgroup comprises monocytes, natural killer cells, B cells, $CD4^+$ T cells, and $CD8^+$ T cells. The Cardiovascular ccf-gDNA fragment-enriched subgroup includes vascular endothelial cells and left atrial cells. Erythrocyte progenitors were considered as their own tissue group since these cells comprise a significant proportion of ccf-gDNA fragments on their own and do not fit into a separate tissue category. The digestive tissue group comprises pancreatic beta, acinar, and duct cells, hepatocytes, colon epithelial cells, bladder cells, kidney cells, and upper gastrointestinal tract cells. The respiratory cells include lung cells and head and larynx cells. Finally, the excluded cell types include neutrophils, thyroid cells, prostate cells, uterus/cervix cells, breast cells, adipocytes, and cortical neurons. Neutrophils were excluded because they comprise a large proportion of the ccf-gDNA and obscure other patient-to-patient differences. The remaining cell types were excluded due to very low occurrence or being a part of sex-dependent organs. (**B**) Hierarchical clustering using the Ward technique and Euclidean distance metric of patient tissue ccf-gDNA signatures. Clustering suggests 3 ccf-gDNA-enriched subgroups: Immune, Cardiovascular, and Erythrocyte progenitor.

Cardiovascular CCF-gDNA Subgroup Has Higher Proportion of Cardiovascular Comorbidities and Frailty

All 3 groups had similar ages and years to death following the ccf-gDNA visit (Figure 2A). Individuals in the CV ccf-gDNA subgroup demonstrated an increased incidence of myocardial infarction, congestive heart failure, and stroke compared to the other groups (Figure 2B). Specifically, they had a greater overall cumulative incidence of individuals with myocardial infarction, congestive heart failure, and stroke compared to the other major ccf-gDNA subgroups at the last study visit (Figure 2B). Thirty-nine percent of participants in the CV ccf-gDNA subgroup had myocardial infarction at the last follow-up visit, compared to 23% of individuals in the Erythrocyte ccf-gDNA subgroup and 21% of individuals in the Immune ccf-gDNA subgroup. A diagnosis of congestive heart failure was noted in 28% of participants in the CV ccf-gDNA subgroup at the last study visit, while 21% and 8% of participants in the Erythrocyte and Immune ccf-gDNA subgroups, respectively, had this diagnosis. Finally, 29% of participants in the CV ccf-gDNA subgroup had a diagnosis of stroke at the last follow-up visit compared to 21% and 20% in the Erythrocyte and Immune ccf-gDNA subgroups, respectively.

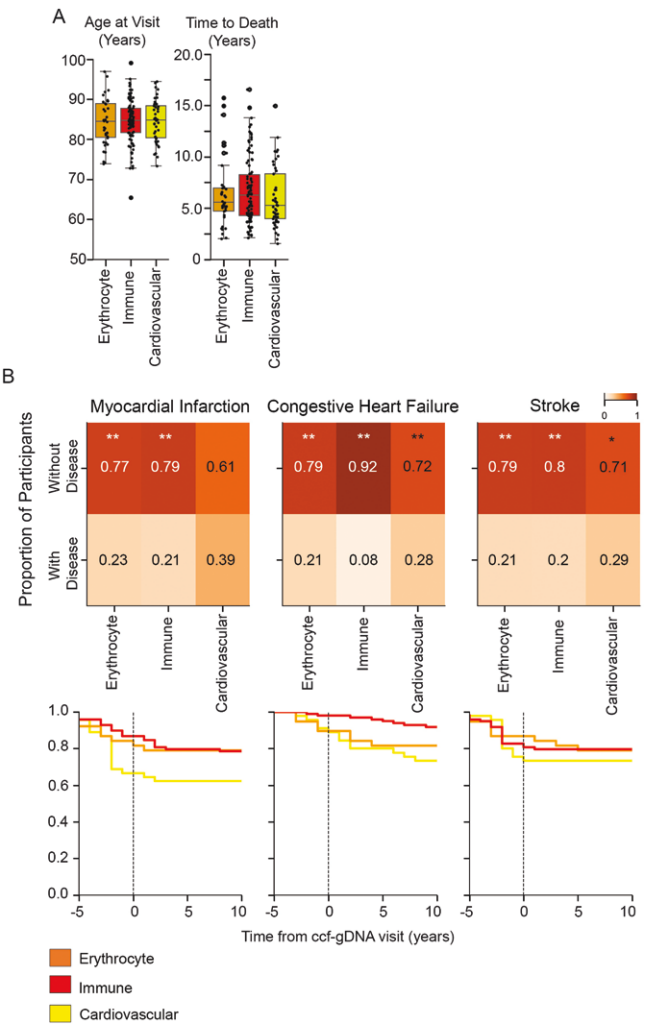

Figure 2. The Cardiovascular circulating cell-free genomic DNA (ccf-gDNA) fragment-enriched subgroup is associated with cardiovascular outcomes. (**A**) Age at study visit across all 3 ccf-gDNA subgroups showing chronological age and time to death, calculated as the years until death from the visit at which ccf-gDNA was collected. (**B**) Proportional breakdown of myocardial infarction, congestive heart failure, and stroke at last follow-up visit (upper heatmaps) and across the study period (lower graphs) for the 3 subgroups. Dashed line on graphs indicates time of ccf-gDNA measurement. $n = 38$ Erythrocyte ccf-gDNA subgroup; $n = 98$ Immune ccf-gDNA subgroup; $n = 45$ Cardiovascular ccf-gDNA subgroup.

Given the established association between cardiovascular morbidity, mortality, and declines in physical and cognitive functions, our analysis next focused on the CV ccf-gDNA subgroup, given their integral role in the broader spectrum of health and aging dynamics. Frailty is an age-related heterogenous syndrome characterized by diminished capacity to respond to physical and psychosocial stressors and is a risk factor for development of major adverse cardiac events (MACEs) (33). The CV ccf-gDNA subgroup had significantly higher frailty scores than the Erythrocyte ccf-gDNA subgroup (Figure 3A). Eighteen percent of participants in the CV ccf-gDNA subgroup and 14% of Immune ccf-gDNA subgroup participants were frail at the time of ccf-gDNA measurement compared to 7% of participants in the Erythrocyte ccf-gDNA subgroup. At the last study visit, 62% of CV ccf-gDNA subgroup participants were frail, compared to 21%

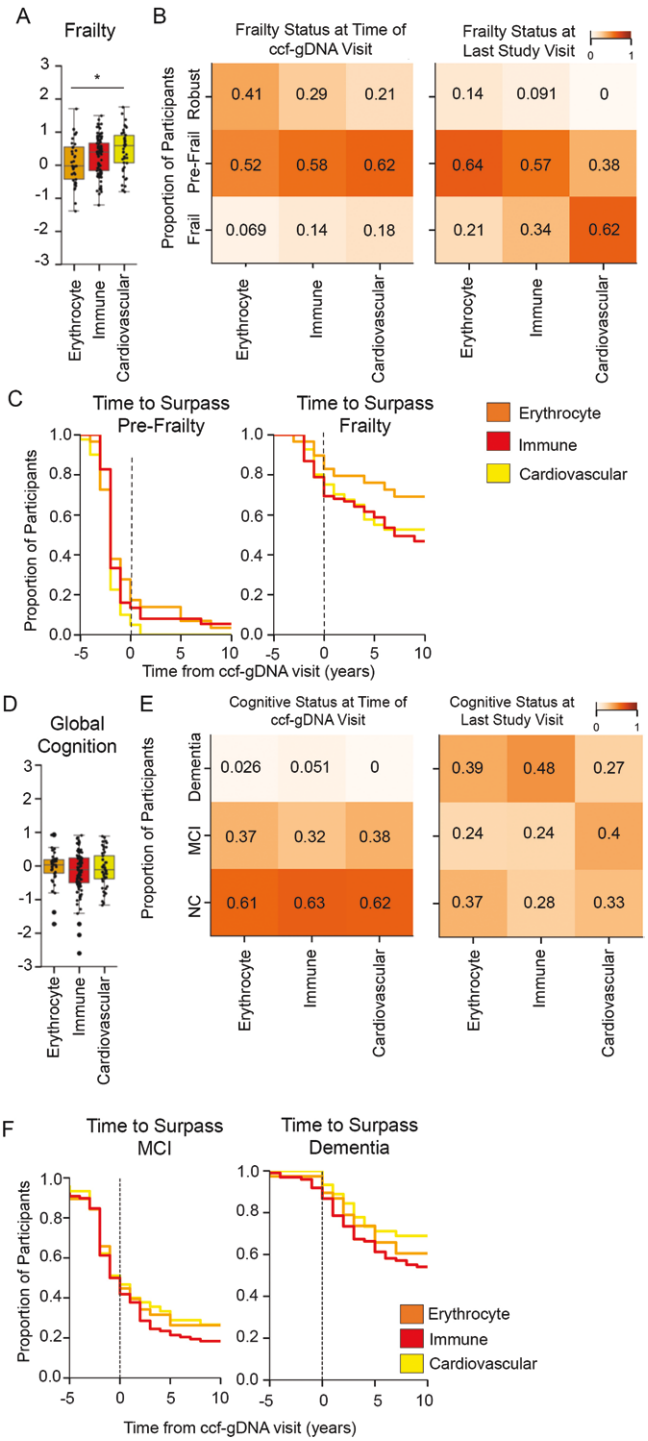

Figure 3. The Cardiovascular circulating cell-free genomic DNA (ccf-gDNA) fragment-enriched subgroup has higher frailty measures compared to other subgroups, and there is no difference in cognitive status across subgroups. (**A**) Continuous frailty scores (*z*-standardized) for all 3 ccf-gDNA subgroups at time of visit at which ccf-gDNA was collected. (**B**) Heatmap demonstrating proportional breakdown of frailty status at time of ccf-gDNA measurement and last follow-up visit. (**C**) Proportion of prefrailty diagnosis and frailty diagnosis across the study period for the 3 subgroups. Dashed line on graphs indicates time of ccf-gDNA measurement. (**D**) Global cognition scores (*z*-standardized) for all 3 ccf-gDNA subgroups at time of visit at which ccf-gDNA was collected. (**E**) Heatmap demonstrating proportional breakdown of cognitive status at time of ccf-gDNA measurement and last follow-up visit. (**F**) Proportion of mild cognitive impairment diagnosis and dementia diagnosis across the study period for the 3 subgroups. Dashed line on graphs indicates time of ccf-gDNA measurement. n = 38 Erythrocyte ccf-gDNA subgroup; n = 98 Immune ccf-gDNA subgroup; n = 45 Cardiovascular ccf-gDNA subgroup. MCI = mild cognitive impairment; NC = normal cognition

of Erythrocyte ccf-gDNA subgroup participants and 34% of Immune ccf-gDNA subgroup participants.

Individuals identified as being in the CV ccf-gDNA subgroup had 3.1 times higher odds of being more frail than individuals in the Erythrocyte ccf-gDNA subgroup when adjusting for age, sex, and ccf-gDNA levels. The CV ccf-gDNA subgroup frailty scores also appeared higher than the Immune ccf-gDNA subgroup, but no significant differences were detected between these 2 groups (Figure 3B and C, Supplementary Figure S3). A similar study of cognitive outcomes among these participants showed no significant differences in global cognitive score across ccf-gDNA subgroups (Figure 3D), and no significant differences across groups at time of ccf-gDNA measurement or at last study visit (Figure 3E and F). There were no significant differences between subgroups for cognition subscores, including perceptual orientation, perceptual speed, semantic memory, working memory, and episodic memory (Supplementary Figure S3).

Epigenetic Age Acceleration of CCF-gDNA Fragments Differs Across Subgroups

Given the similar chronological ages across our identified ccf-gDNA subgroups, we turned our attention to exploring variations in biological age of the ccf-gDNA fragments, specifically whether epigenetic age estimates from DNAm patterns of ccf-gDNA were comparable to those derived from living cells (CD4 T cells) in this older adult population. As shown in Table 2, zero-order correlations demonstrate weak associations ($p < .05$) between the epigenetic clocks and chronological age at the relevant study visit. Notably, correlations between the CD4-derived epigenetic clocks were larger in magnitude compared to the correlations among the ccf-gDNA derived epigenetic clocks.

We also examined the variability in biological age derived from the circulating ccf-gDNA fragments among the CV, Immune, and Erythrocyte ccf-gDNA subgroups. Using multivariable linear regression, we empirically tested whether epigenetic age acceleration estimates were comparable between methylation data derived from ccf-gDNA and CD4 cells, adjusting for the time between the ccf-gDNA and CD4 sample visits. Our findings demonstrate that ccf-gDNA Hannum and GrimAge acceleration estimates are associated with the same estimates from CD4 cells (β = 0.26, 95% confidence interval [CI] = 0.09–0.43, $p = .003$ and β = 0.18, 95% CI = 0.02–0.34, $p = .03$, respectively).

Using the 3 ccf-gDNA subgroups identified by hierarchical clustering, results from linear regression models revealed that membership in either the Erythrocyte ccf-gDNA (β = −3.11, $SE = 1.21$, $p = .01$) or Immune ccf-gDNA (β = −3.32, $SE = 0.99$, $p = .001$) subgroup was associated with an approximately 3-year decrease in GrimAge acceleration relative to the CV ccf-gDNA subgroup (Figure 4). Similarly, assignment to the Immune ccf-gDNA subgroup was associated with an approximately 3.5-year decrease in Hannum age acceleration relative to the CV ccf-gDNA subgroup (β = −3.60, $SE = 1.28$, $p = .01$). No other significant associations were detected.

In summary, our findings indicate that (i) epigenetic age estimates calculated from ccf-gDNA are, in general, correlated

Table 2. Zero-Order Correlations Among Epigenetic Clocks Derived From CCF-gDNA (n = 181) and CD4 Cells (n = 39), With Chronological Age, at Index Visit

	1.	2.	3.	4.
1. Chronological Age	–			
2. ccf-gDNA Hannum	**0.48**	–		
3. ccf-gDNA GrimAge	**0.46**	**0.42**	–	
4. CD4 Hannum	**0.58**	**0.33**	**0.42**	–
5. CD4 GrimAge	**0.84**	**0.37**	**0.55**	**0.56**

Notes: ccf-gDNA = circulating cell-free genomic DNA fragments. Bold values reflect correlations with p-values <.05. Because the ccf-gDNA samples were not all collected at the same time as the CD4 samples, the chronological age variable (ie, age at visit) varies between the ccf-gDNA and CD4 epigenetic clocks.

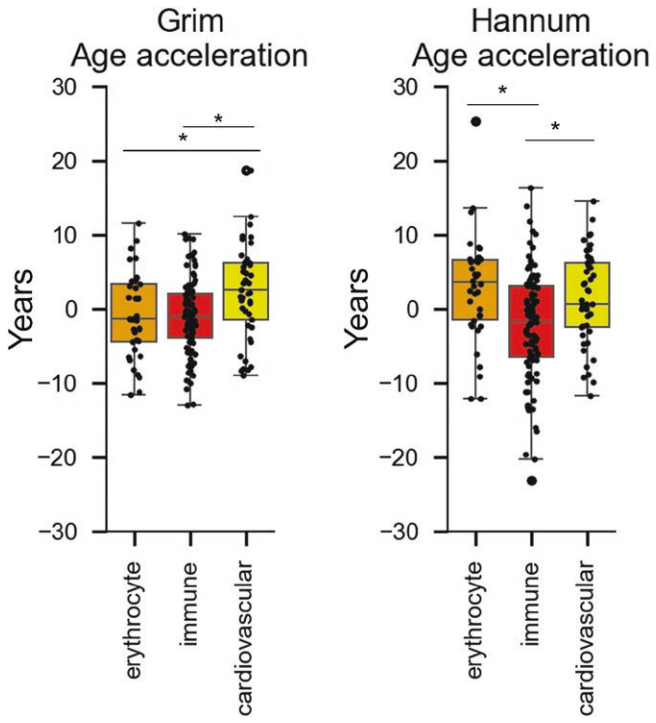

Figure 4. The Cardiovascular circulating cell-free genomic DNA (ccf-gDNA) fragment-enriched subgroup has increased age acceleration compared to the other subgroups. Calculated GrimAge acceleration and Hannum age acceleration across subgroups. N = 38 Erythrocyte ccf-gDNA subgroup; N = 98 Immune ccf-gDNA subgroup; N = 45 Cardiovascular ccf-gDNA subgroup.

with estimates derived from living cells in older adults and (ii) assignment to the CV ccf-gDNA subgroup is associated with accelerated epigenetic aging, as indicated by GrimAge and Hannum age estimates.

Examining the Links Between the Circulating Metabolome and Tissue Source of ccf-gDNA Fragments

We next studied the circulating metabolome to further characterize the ccf-gDNA tissue subgroups identified by hierarchical clustering. Given the differences in frailty and cardiovascular disease between the CV ccf-gDNA subgroup compared to the immune and erythrocyte subgroups, we sought to identify differences in energy utilization between these groups. As a directly measurable marker of cell metabolic processes, integrating serum metabolomics with epigenetics approaches to measure biological age and age acceleration can provide additional information about lifestyle risk factors for premature mortality (34,35). Targeted approaches were used to analyze a range of metabolites in the serum samples and identify specific metabolic signatures associated with the tissue of origin and organ system for ccf-gDNA.

We performed a metabolite set enrichment analysis to identify enriched pathways between the 3 ccf-gDNA subgroups derived from hierarchical clustering. Several metabolic pathways were enriched in the CV ccf-gDNA subgroup in comparison to the Immune and Erythrocyte ccf-gDNA enriched subgroups (Figure 5A). These pathways predominantly include amino acid and lipid metabolic pathways. Metabolomics analysis highlighted notable variations in several metabolites and pathways across groups, with the most pronounced dysregulation observed in the urea cycle (Figure 5B) and glycine/serine metabolic pathway (Figure 5C) within the CV ccf-gDNA subgroup, as compared to both the Immune and Erythrocyte ccf-gDNA subgroups. Several metabolites within the urea cycle appear to be upregulated in the CV ccf-gDNA subgroup, as seen by positive log fold changes, when compared to the other 2 subgroups. Within the glycine/serine pathway, several metabolites are either up- or downregulated in the CV ccf-gDNA subgroup when compared to the other 2 subgroups, and the directionality of this change is always the same compared to the other 2 subgroups.

Supplementary Tables S1 and S2 show distinct metabolite profiles that are correlated with different tissue and organ sources for ccf-gDNA fragments. The results of these analyses indicate that the metabolite profiles differ for the 3 main ccf-gDNA groups, although the CV ccf-gDNA subgroup appears to be most different from the other 2 groups.

Discussion

This study provides a multifaceted view of aging through the analysis of ccf-gDNA in older adults, combining epigenetics and metabolomics to link ccf-gDNA tissue origins with epigenetic aging and clinical outcomes. Circulating cell-free DNA fragments have shown promise as potential biomarkers for many diseases, including cancer diagnostics and noninvasive fetal screening. In this study, 3 distinct subgroups of individuals were identified based on ccf-gDNA tissue of origin, and we found associations with the CV ccf-gDNA subgroup and cardiovascular disease outcomes as well as with higher rates of frailty. We did not note any associations with ccf-gDNA tissue of origin and cognitive test scores. Further analysis revealed variability in epigenetic age across subgroups, with

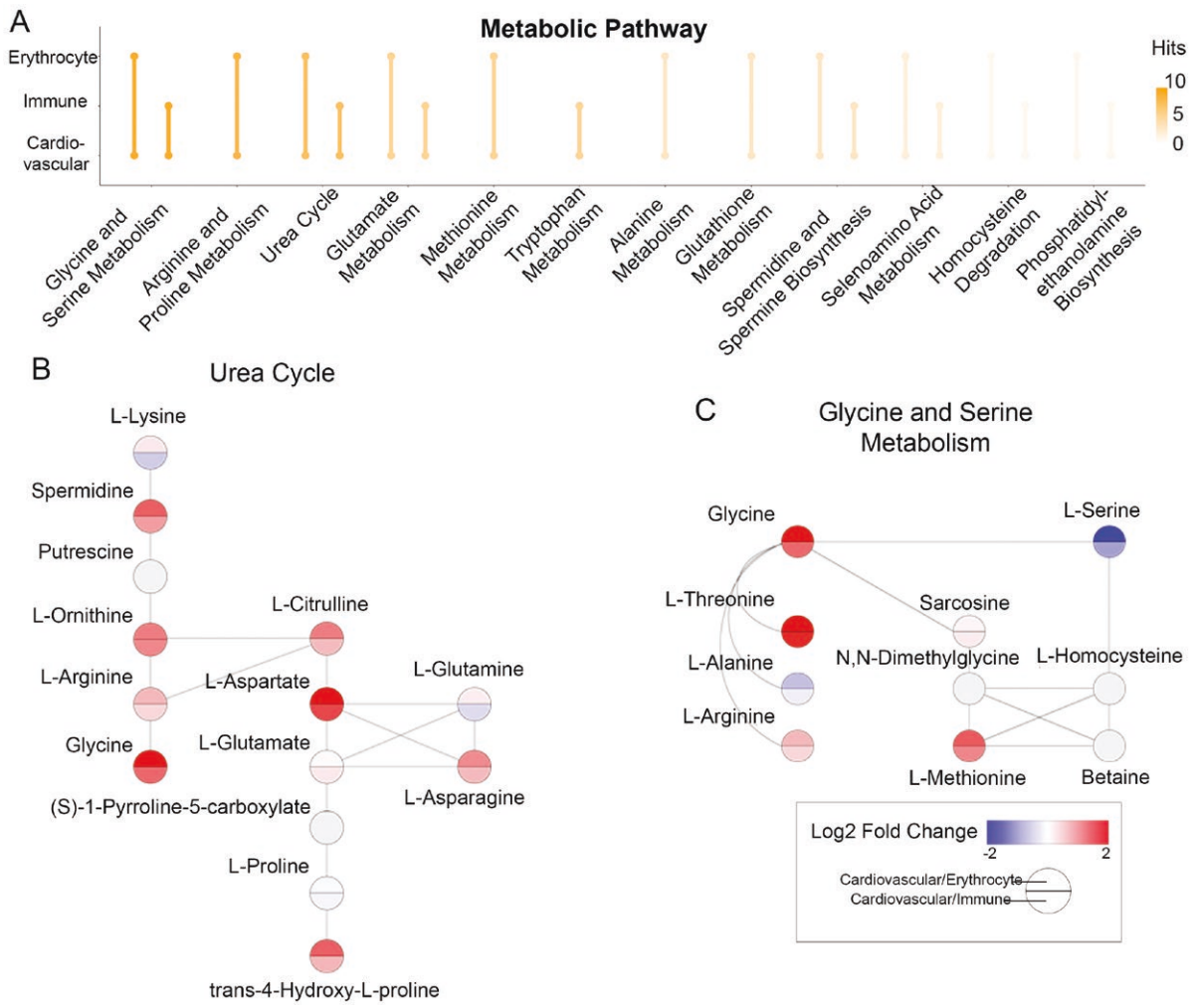

Figure 5. Identification of metabolic signatures associated with each circulating cell-free genomic DNA (ccf-gDNA) group. (**A**) Metabolite set enrichment analysis demonstrates enriched metabolic pathways when conducting pairwise comparisons between Cardiovascular and Erythrocyte or Cardiovascular and Immune ccf-gDNA subgroups. No common pathways were enriched between Erythrocyte and Immune ccf-gDNA subgroups. (**B**) Schematic of the urea cycle and enriched metabolites in this study. (**C**) A simplified schematic of the glycine and serine metabolism pathway with indication of which metabolites are enriched.

the CV ccf-gDNA subgroup demonstrating greater epigenetic age acceleration, pointing to ccf-gDNA as a potential holistic marker of biological aging. Metabolomic analysis supported these findings by highlighting specific metabolic pathways associated with each subgroup, especially the CV ccf-gDNA subgroup, underscoring the metabolic basis of aging and disease risk.

This work found that most ccf-gDNA fragments originated from neutrophils, consistent with previous studies (15), and showed the feasibility of tissue deconvolution using smaller sample volumes than in prior studies. A prior study purified cf-DNA from 6 mL of plasma before performing EPIC array methylation analysis (11), while our study required only 450 µL total serum. Our findings provide new insights into using ccf-gDNA as a potential biomarker for monitoring physical health and cardiovascular disease in older adults. Frailty remains a critical indicator of health that has stronger associations with morbidity and mortality than age alone (36). Frailty is a state of increased vulnerability to adverse health outcomes resulting from a decline in physiological reserves and function across multiple organ systems and is characterized by diminished strength and endurance. The frailty phenotype was first operationalized using participants in the Cardiovascular Health Study, a prospective observational study focused on identifying incident risk factors for developing cardiovascular disease in older adults (37), and a companion study published in the same cohort of individuals showed that 38% of individuals classified as frail had a diagnosis of cardiovascular disease (38).

More recently, large prospective cohort studies have established a link between frailty and increased incidence of developing major adverse cardiovascular events and found increased hazard of developing myocardial infarction (hazard ratio [HR] 1.95), coronary artery disease (HR 1.35), and stroke (HR 1.71) (33), which are 3 outcomes that we found to be higher in participants in the CV ccf-gDNA subgroup. This relationship between frailty and cardiovascular disease is hypothesized to be bidirectional, given the overlap in molecular and physiologic drivers for both conditions, which include mitochondrial dysfunction, cell death, senescence, and dysregulated metabolic systems (37,39).

The Immune ccf-gDNA subgroup, consisting of individuals with ccf-gDNA originating from monocytes, B cells, T cells, and natural killer cells, demonstrated lower total WBC counts

compared to the other 2 subgroups, and a possible hypothesis for this association could be due to increased WBC death and consequent ccf-gDNA fragment production, possibly from increases in neutrophil extracellular traps (NETs) in these individuals. Future studies measuring complete differential WBC counts for participants can confirm if there are inverse relationships between T cells, monocytes, and immune cell ccf-gDNA. This study showed no associations between the Erythrocyte ccf-gDNA subgroup and laboratory measures of hemoglobin; however, we cannot rule out that our study may be underpowered for this outcome.

We found weakly positive correlations between age acceleration estimates between calculated DNAm Age using ccf-gDNA fragments and Hannum and GrimAge clocks using methylation data from living CD4 T cells. Measuring the biological age of ccf-gDNA fragments can convey different information regarding an individual's biological age compared to CD4 T-cell-derived biological age due to it originating from various tissues. There have been recent efforts to develop ccf-gDNA-based aging clocks, such as the one from Shtumpf et al., which predicts chronologic age based on age-related changes in nucleosome organization resulting in longer distances between nucleosomes (40). Our study did not sequence ccf-gDNA fragments and focused on quantifying amounts of ccf-gDNA originating from different tissues. Future studies can combine these analytic approaches to better understand changes in ccf-gDNA with aging and examine whether altered nucleosome organization also varies by tissue type of origin. It may be that combining the 2 measures is most informative by incorporating the biological age of living cells from CD4-derived clocks and the biological age of fragments released in circulation; however, the relatively small sample size in this study is a limiting factor in performing these analyses but can be examined in follow-up studies with larger sample sizes. Given the associations with CV ccf-gDNA subgroup, increased frailty and cardiovascular disease, and higher biological age, it may be detrimental to have higher levels of older fragments in circulation, which could be a byproduct of inefficient or dysfunctional cellular repair processes.

Metabolomics results demonstrate that CV ccf-gDNA subgroup has a distinct metabolomic profile when compared to the immune and erythrocyte subgroups. Urea cycle-associated metabolites (aspartate, arginine, and hydroxyproline) were enriched in CV ccf-gDNA participant serum compared to others. Additionally, glycine/serine metabolic pathways demonstrated dysregulation in metabolomic analysis for CV ccf-gDNA subgroup, specifically for glycine, threonine, and methionine (all increased), and serine (decreased). When comparing our findings to the literature, there are some inconsistencies in the trends we observe. Firstly, elevations in serine were recently shown to be associated with reduced prevalence of coronary artery disease in hospitalized patients, and our study showing decreased levels of serine in serum is consistent with the increased prevalence of developing cardiovascular disease seen in the CV ccf-gDNA subgroup (41). Elevated glycine in plasma is associated with a lower hazard of developing hypertension, a risk factor for both congestive heart disease and stroke (42). Increased methionine is associated with heart failure with preserved ejection fraction, a subtype of heart failure that older adults are at higher risk of developing (43).

Several limitations when attempting to directly compare the metabolic results from this study with other cardiovascular disease-focused studies are the differences in the material studied (serum vs plasma), study sample size, follow-up period, and sex and age of their study population. Additionally, the parent ROS-MAP study may have recruited more healthy older adults compared to these other studies, and there could be a component of survivorship bias that is leading to the differences in metabolomics findings.

Recent work incorporating metabolomics datasets to develop biological clocks demonstrate the ability to generate risk profiles for individuals (34,44), and our study demonstrates feasibility of developing multilayered biologic clocks using metabolomics and epigenetic clock data generated from banked patient serum.

Our study's strengths include using novel methodology to estimate tissue of origin of ccf-gDNA fragments in older individuals, standardized measures to capture multiple aspects of cognitive and physical functioning, and the longitudinal nature of the data that allows for understanding these associations over time. Additionally, the ability to identify subpopulations of frailty based on ccf-gDNA source opens new avenues of study to further characterize this heterogenous syndrome and apply precision-medicine-based interventions that are developed to benefit certain subgroups with frailty. The study is also strengthened by including DNAm data from living cells, allowing us to compare epigenetic age estimates between 2 different cell states (ie, living vs dead). However, the study's limitations include the small sample size, which may have impacted the statistical power of this study, contributing to null results for cognitive outcomes.

This study utilizes serum samples collected as part of the longitudinal ROS-MAP study. However, there are limitations when studying ccf-gDNA from serum samples, specifically an overestimation of cell-free DNA levels in serum samples compared to plasma due to contamination of circulating cf-DNA with DNA originating from WBCs as part of serum processing methods (45). Excluding neutrophils from clustering analysis, as we did in this study, is one way to minimize the outsized contribution of WBC DNA contaminating circulating ccf-gDNA in serum samples, but it also limits the conclusions of this study by excluding the predominant source of ccf-gDNA fragments. Neutrophil-derived ccf-gDNA fragments can also be generated from NETosis, a process that is present in cardiovascular diseases and can contribute to atherosclerotic plaque formation (46). Future work can specifically study relationships between NETosis, neutrophil-derived circulating ccf-gDNA, and physical and cognitive decline in older adults. Another limitation is the inability to determine how ccf-gDNA estimates changed as individuals aged and the lack of a validation test of actual neuronal cell counts in the same individuals to assess whether ccf-gDNA estimates of cortical neurons reflect actual neuronal loss.

Our prior work has shown associations between ccf-gDNA and cognitive score trajectories, and high levels of ccf-gDNA were associated with an increased hazard of developing a dementia diagnosis over an 8-year period. Although this prior study also showed associations between ccf-gDNA and steeper frailty trajectories, and we did find associations with ccf-gDNA tissue of origin and frailty status, we did not see significant differences across the 3 ccf-gDNA tissue of origin subgroups for either cognitive diagnosis or cognitive test score. Thirty-eight percent of participants in this study developed a diagnosis of dementia at the last study visit, and our findings show no associations between cognitive test scores or clinical diagnosis of cognitive status and major ccf-gDNA

subgroups identified in this study. An additional factor that may have resulted in null findings for ccf-gDNA of origin and cognitive outcomes is that among the participants in this study, there was a very low percentage of ccf-gDNA originating from cortical neurons (0.3%). Given that the one-time assessment of ccf-gDNA in this study was done early in the course of ROS-MAP enrollment for these participants, future studies can examine ccf-g DNAm at later timepoints, such as at the time of conversion from normal cognition to MCI to see if at this later timepoint there are associations between cognitive outcomes and ccf-gDNA tissue of origin.

This study shows that characterizing ccf-gDNA tissue of origin can identify individuals that have higher rates of cardiovascular events, particularly myocardial infarction, stroke, and congestive heart failure. Individuals with higher levels of cardiovascular-derived ccf-gDNA also have ccf-gDNA that has a higher biological age, indicating that they originated from older cells. Our findings provide new insights into developing methods for biochemical characterization of frailty subtypes using cell-free DNA.

Supplementary Material

Supplementary data are available at *The Journals of Gerontology, Series A: Biological Sciences and Medical Sciences* online.

Funding

This study was supported by the Johns Hopkins Older Americans Independence Center National Institute on Aging (P30AG021334), the National Institute on Aging grant K24AG088484 (P.M.A.), the National Institute on Aging (T32AG058527) Translational Aging Research Training Program, the National Institute on Aging grants R03AG078924 and K23AG084877 (L.S.N.), the National Institute of Mental Health DA047064 (D.W.S. and B.S.M.), the AFAR Grants for Junior Faculty (J.M.P.), and the National Institutes of Health Shared Instrument Grant-S10 (1S10OD025226-01, A.L.). ROS-MAP is supported by P30AG10161, P30AG72975, R01AG15819, R01AG17917, U01AG46152, and U01AG61356 (D.A.B.).

Conflict of Interest

None.

Data Availability

ROS-MAP resources can be requested at https://www.radc.rush.edu and https://www.synpase.org.

Acknowledgments

We thank Roxann Ashworth and the team at the Johns Hopkins University School of Medicine Genetic Resources Core Facility (RRID:SCR_018669).

References

1. López-Otín C, Blasco MA, Partridge L, Serrano M, Kroemer G. The hallmarks of aging. *Cell*. 2013;153:1194–1217. https://doi.org/10.1016/j.cell.2013.05.039
2. Levine B, Kroemer G. Autophagy in aging, disease and death: The true identity of a cell death impostor. *Cell Death Differ*. 2009;16:1–2. https://doi.org/10.1038/cdd.2008.139
3. Tower J. Programmed cell death in aging. *Ageing Res Rev*. 2015;23:90–100. https://doi.org/10.1016/j.arr.2015.04.002
4. Monti D, Troiano L, Tropea F, et al. Apoptosis—programmed cell death: A role in the aging process? *Am J Clin Nutr*. 1992;55:1208S–1214S. https://doi.org/10.1093/ajcn/55.6.1208S
5. Martin LJ. Mitochondrial and cell death mechanisms in neurodegenerative diseases. *Pharmaceuticals (Basel)*. 2010;3:839–915. https://doi.org/10.3390/ph3040839
6. Mulero J, Zafrilla P, Martinez-Cacha A. Oxidative stress, frailty and cognitive decline. *J Nutr Health Aging*. 2011;15:756–760. https://doi.org/10.1007/s12603-011-0130-5
7. Kustanovich A, Schwartz R, Peretz T, Grinshpun A. Life and death of circulating cell-free DNA. *Cancer Biol Ther*. 2019;20:1057–1067. https://doi.org/10.1080/15384047.2019.1598759
8. Park SS, Jeong H, Andreazza AC. Circulating cell-free mitochondrial DNA in brain health and disease: A systematic review and meta-analysis. *World J Biol Psychiatry*. 2022;23:87–102. https://doi.org/10.1080/15622975.2021.1938214
9. Liu S, Wang J. Current and future perspectives of cell-free DNA in liquid biopsy. *Curr Issues Mol Biol*. 2022;44:2695–2709. https://doi.org/10.3390/cimb44060184
10. Nidadavolu LS, Feger D, Wu Y, et al. Circulating cell-free genomic DNA is associated with an increased risk of dementia and with change in cognitive and physical function. *J Alzheimers Dis*. 2022;89:1233–1240. https://doi.org/10.3233/JAD-220301
11. Bahado-Singh RO, Radhakrishna U, Gordevičius J, et al. Artificial intelligence and circulating cell-free DNA methylation profiling: Mechanism and detection of Alzheimer's disease. *Cells*. 2022;11:1744. https://doi.org/10.3390/cells11111744
12. Lehmann-Werman R, Neiman D, Zemmour H, et al. Identification of tissue-specific cell death using methylation patterns of circulating DNA. *Proc Natl Acad Sci USA*. 2016;113:E1826–E1834. https://doi.org/10.1073/pnas.1519286113
13. Guo S, Diep D, Plongthongkum N, Fung H-L, Zhang K, Zhang K. Identification of methylation haplotype blocks aids in deconvolution of heterogeneous tissue samples and tumor tissue-of-origin mapping from plasma DNA. *Nat Genet*. 2017;49:635–642. https://doi.org/10.1038/ng.3805
14. Snyder MW, Kircher M, Hill AJ, Daza RM, Shendure J. Cell-free DNA comprises an in vivo nucleosome footprint that informs its tissues-of-origin. *Cell*. 2016;164:57–68. https://doi.org/10.1016/j.cell.2015.11.050
15. Moss J, Magenheim J, Neiman D, et al. Comprehensive human cell-type methylation atlas reveals origins of circulating cell-free DNA in health and disease. *Nat Commun*. 2018;9:5068. https://doi.org/10.1038/s41467-018-07466-6
16. Bell CG, Lowe R, Adams PD, et al. DNA methylation aging clocks: Challenges and recommendations. *Genome Biol*. 2019;20:249. https://doi.org/10.1186/s13059-019-1824-y
17. Bocklandt S, Lin W, Sehl ME, et al. Epigenetic predictor of age. *PLoS One*. 2011;6:e14821. https://doi.org/10.1371/journal.pone.0014821
18. Hannum G, Guinney J, Zhao L, et al. Genome-wide methylation profiles reveal quantitative views of human aging rates. *Mol Cell*. 2013;49:359–367. https://doi.org/10.1016/j.molcel.2012.10.016
19. Duan R, Fu Q, Sun Y, Li Q. Epigenetic clock: A promising biomarker and practical tool in aging. *Ageing Res Rev*. 2022;81:101743. https://doi.org/10.1016/j.arr.2022.101743
20. Lu AT, Quach A, Wilson JG, et al. DNA methylation GrimAge strongly predicts lifespan and healthspan. *Aging (Albany NY)*. 2019;11:303–327. https://doi.org/10.18632/aging.101684
21. McCrory C, Fiorito G, Hernandez B, et al. GrimAge outperforms other epigenetic clocks in the prediction of age-related clinical phenotypes and all-cause mortality. *J Gerontol A Biol Sci Med Sci*. 2021;76:741–749. https://doi.org/10.1093/gerona/glaa286

22. Bennett DA, Schneider JA, Arvanitakis Z, Wilson RS. Overview and findings from the Religious Orders Study. *Curr Alzheimer Res*. 2012;9:628–645. https://doi.org/10.2174/156720512801322573
23. Bennett DA, Buchman AS, Boyle PA, Barnes LL, Wilson RS, Schneider JA. Religious Orders Study and Rush Memory and Aging Project. *J Alzheimers Dis*. 2018;64:S161–S189. https://doi.org/10.3233/JAD-179939
24. Pidsley R, Zotenko E, Peters TJ, et al. Critical evaluation of the Illumina MethylationEPIC BeadChip microarray for whole-genome DNA methylation profiling. *Genome Biol*. 2016;17:208. https://doi.org/10.1186/s13059-016-1066-1
25. Yu L, Chibnik LB, Yang J, et al. Methylation profiles in peripheral blood CD4⁺ lymphocytes versus brain: The relation to Alzheimer's disease pathology. *Alzheimers Dement*. 2016;12:942–951. https://doi.org/10.1016/j.jalz.2016.02.009
26. Wilson RS, Boyle PA, Yu L, et al. Temporal course and pathologic basis of unawareness of memory loss in dementia. *Neurology*. 2015;85:984–991. https://doi.org/10.1212/WNL.0000000000001935
27. Bennett DA, Schneider JA, Arvanitakis Z, et al. Neuropathology of older persons without cognitive impairment from two community-based studies. *Neurology*. 2006;66:1837–1844. https://doi.org/10.1212/01.wnl.0000219668.47116.e6
28. Bennett DA, Wilson RS, Schneider JA, et al. Natural history of mild cognitive impairment in older persons. *Neurology*. 2002;59:198–205. https://doi.org/10.1212/wnl.59.2.198
29. Bennett DA, Schneider JA, Aggarwal NT, et al. Decision rules guiding the clinical diagnosis of Alzheimer's disease in two community-based cohort studies compared to standard practice in a clinic-based cohort study. *Neuroepidemiology*. 2006;27:169–176. https://doi.org/10.1159/000096129
30. Buchman AS, Wilson RS, Bienias JL, Bennett DA. Change in frailty and risk of death in older persons. *Exp Aging Res*. 2009;35:61–82. https://doi.org/10.1080/03610730802545051
31. Buchman AS, Boyle PA, Wilson RS, Tang Y, Bennett DA. Frailty is associated with incident Alzheimer's disease and cognitive decline in the elderly. *Psychosom Med*. 2007;69:483–489. https://doi.org/10.1097/psy.0b013e318068de1d
32. Chong J, Wishart DS, Xia J. Using MetaboAnalyst 4.0 for comprehensive and integrative metabolomics data analysis. *Curr Protoc Bioinform*. 2019;68:e86. https://doi.org/10.1002/cpbi.86
33. Damluji AA, Chung S-E, Xue Q-L, et al. Frailty and cardiovascular outcomes in the National Health and Aging Trends Study. *Eur Heart J*. 2021;42:3856–3865. https://doi.org/10.1093/eurheartj/ehab468
34. Robinson O, Chadeau Hyam M, Karaman I, et al. Determinants of accelerated metabolomic and epigenetic aging in a UK cohort. *Aging Cell*. 2020;19:e13149. https://doi.org/10.1111/acel.13149
35. Kuiper LM, Polinder-Bos HA, Bizzarri D, et al. Epigenetic and metabolomic biomarkers for biological age: A comparative analysis of mortality and frailty risk. *J Gerontol A Biol Sci Med Sci*. 2023;78:1753–1762. https://doi.org/10.1093/gerona/glad137
36. Hoogendijk EO, Afilalo J, Ensrud KE, Kowal P, Onder G, Fried LP. Frailty: Implications for clinical practice and public health. *Lancet*. 2019;394:1365–1375. https://doi.org/10.1016/S0140-6736(19)31786-6
37. Fried LP, Tangen CM, Walston J, et al.; Cardiovascular Health Study Collaborative Research Group. Frailty in older adults: Evidence for a phenotype. *J Gerontol A Biol Sci Med Sci*. 2001;56:M146–M156. https://doi.org/10.1093/gerona/56.3.m146
38. Newman AB, Gottdiener JS, Mcburnie MA, et al.; Cardiovascular Health Study Research Group. Associations of subclinical cardiovascular disease with frailty. *J Gerontol A Biol Sci Med Sci*. 2001;56:M158–M166. https://doi.org/10.1093/gerona/56.3.m158
39. Ijaz N, Buta B, Xue Q-L, et al. Interventions for frailty among older adults with cardiovascular disease: JACC state-of-the-art review. *J Am Coll Cardiol*. 2022;79:482–503. https://doi.org/10.1016/j.jacc.2021.11.029
40. Shtumpf M, Jeong S, Bikova M, Mamayusupova H, Ruje L, Teif VB. Aging clock based on nucleosome reorganisation derived from cell-free DNA. *Aging Cell*. 2024;23:e14100. https://doi.org/10.1111/acel.14100
41. Fan F, Liang Z, Liu Z, et al. Association between serine concentration and coronary heart disease: A case-control study. *Int J Gen Med*. 2024;17:2955–2965. https://doi.org/10.2147/IJGM.S467320
42. Dziedzic M, Józefczuk E, Guzik TJ, Siedlinski M. Interplay between plasma glycine and branched-chain amino acids contributes to the development of hypertension and coronary heart disease. *Hypertension*. 2024;81:1320–1331. https://doi.org/10.1161/HYPERTENSIONAHA.123.22649
43. Razavi AC, Bazzano LA, He J, et al. Novel findings from a metabolomics study of left ventricular diastolic function: The Bogalusa Heart Study. *J Am Heart Assoc*. 2020;9:e015118. https://doi.org/10.1161/JAHA.119.015118
44. van den Akker EB, Trompet S, Barkey Wolf JJH, et al. Metabolic age based on the BBMRI-NL ¹H-NMR metabolomics repository as biomarker of age-related disease. *Circ Genom Precis Med*. 2020;13:541–547. https://doi.org/10.1161/CIRCGEN.119.002610
45. Wong FCK, Sun K, Jiang P, et al. Cell-free DNA in maternal plasma and serum: A comparison of quantity, quality and tissue origin using genomic and epigenomic approaches. *Clin Biochem*. 2016;49:1379–1386. https://doi.org/10.1016/j.clinbiochem.2016.09.009
46. Klopf J, Brostjan C, Eilenberg W, Neumayer C. Neutrophil extracellular traps and their implications in cardiovascular and inflammatory disease. *Int J Mol Sci*. 2021;22:559. https://doi.org/10.3390/ijms22020559